Improved Position Observer Using Adaptive Training Control-Based Filter for Interior Permanent Magnet Synchronous Motor Drives

Xuan Wu, Dan Yang, Xu Yu, Kaiyuan Lu, *Member, IEEE*, Ting Wu, Shoudao Huang, *Senior Member, IEEE*, and Hesong Cui

***Abstract*—Rotor position is the key information to achieve superior performance for sensorless control of interior permanent magnet synchronous motor (IPMSM). Nevertheless, the back electromotive force (EMF) model-based position estimation suffers from severe contamination from the fifth and seventh harmonics resulting from inverter nonlinearity and flux spatial harmonics. Therefore, an adaptive training control-based adaptive filter combined with a sliding-mode observer (SMO) is presented for harmonics rejection in the estimated back-EMF, thus improving the rotor position estimation performance. This method, based on the steepest descent algorithm, is capable of self-adjusting harmonic coefficients to obtain the fundamental component online under various frequency conditions adaptively. Additionally, the proposed method has a simpler structure and less calculation burden since its reference signal is self-generated without external injection compared to the conventional method. The effectiveness is verified by experiments at a 1.5-kW IPMSM drive platform.**

***Index Terms*—Adaptive training control, interior permanent magnet synchronous motor (IPMSM), position estimation, sensorless, sliding mode observer (SMO).**

I. Introduction

INTERIOR permanent magnet synchronous motors (IPMSMs) are attractive for various applications in the industry owing to their outstanding performance of high torque density and efficiency [1], [2], [3], [4], [5], [6], [7], [8]. Accurate rotor position information is valuable in the IPMSM control system, whereas a mechanical position sensor may result in many problems, such as increased cost, reduced stability, and so on. Therefore, researches have been reported about the position and speed estimation techniques to achieve sensorless control [9], [10], [11], [12], [13], [14], [15], [16], [17], [18], [19], [20]. However, with the increasing requirements on control performance, estimation accuracy in steady state and dynamic situations have to be guaranteed.

The position estimation methods in sensorless PMSM drives are normally divided into two main categories dependent on motor running speed, that is, high-frequency injection methods [9], [10], [11], [12], [13], [14] and back electromotive force (EMF)-based methods [15], [16], [17], [18], [19], [20]. For high-frequency injection methods, which are suitable for low-speed domain and until the amplitude of back-EMF becomes obvious to be detected, the back-EMF-based methods are adopted for medium and high-speed domains. In which, the back-EMF model-based position estimation methods mainly consist of sliding mode observer (SMO), disturbance observer, state observer, extended Kalman filters, and model reference adaptive systems, etc. Compared to other methods, the SMO is becoming proverbially popular in sensorless IPMSM control systems due to its competitive strengths of robustness against perturbations variation, low sensitivity to parameter variations, and good dynamic performance [17], [18], [19], [20].

Nevertheless, the back-EMF estimates are easily contaminated due to the impacts of the inverter nonlinearity and the flux spatial harmonics, resulting in periodically oscillating position estimation error. The solutions to the above-mentioned problem are mainly categorized into voltage error compensation method and harmonic rejection method. As for voltage error compensation method, some research works have been concentrated on moderating inverter nonlinearity effects [21], [22], [23], [24], [25]. A trapezoidal voltage is created for compensating voltage error caused by inverter nonlinearity to improve motor control performance in [21] and [22]. In [23], an effective parameter-irrelevant compensation approach is used to lower the adverse influence of the current distortion. In [24], a disturbance observer is utilized to estimate the voltage difference to achieve feedforward compensation to neutralize the inverter nonlinearity. However, almost inverter nonlinearity compensation methods ignore the influences of flux spatial harmonics, which will also cause the distortion of the estimated position or even sensorless IPMSM drives failure. In [25], a method considering the flux

Manuscript received 20 August 2022; revised 2 January 2023 and 29 March 2023; accepted 22 May 2023. Date of publication 26 May 2023; date of current version 21 June 2023. This work was supported by the National Natural Science Foundation of China under Grant 52077065. Recommended for publication by Associate Editor H. Hofmann. *(Corresponding author: Dan Yang.)*

Xuan Wu, Dan Yang, Xu Yu, and Shoudao Huang are with the College of Electrical and Information Engineering, Hunan University, Hunan 410006, China (e-mail: wuxuan@hnu.edu.cn; yangdan99@hnu.edu.cn; yuxu98@hnu.edu.cn; hsd1962@hnu.edu.cn).

Kaiyuan Lu is with the Department of Energy Technology, Aalborg University, 9100 Aalborg, Denmark (e-mail: klu@et.aau.dk).

Ting Wu is with the School of Electronic Information, Hunan First Normal University, Hunan 410205, China (e-mail: wting_tata@163.com).

Hesong Cui is with the Machinery Industry Beijing Electrotechnical Institute of Economic Research, Beijing 100070, China (e-mail: cuihesong@hnu.edu.cn).

Color versions of one or more figures in this article are available at https://doi.org/10.1109/TPEL.2023.3280254.

Digital Object Identifier 10.1109/TPEL.2023.3280254

spatial harmonics is proposed to solve nonideal air-gap magnetic field effect by analyzing the back-EMF offline, which will complicate the implementation process and is hard to realize. Summarizing the aforementioned references, voltage error compensation methods can't remove harmonics contained in the rotor position and speed estimation completely. Therefore, in this article, the attention is paid to harmonic rejection method, which can directly extract fundamental back-EMF to ensure position estimation accuracy.

The harmonic rejection method [19], [26], [27], [28], [29], [30] is recognized as an effective method to acquire the smooth rotor information by eliminating harmonic influence, which commonly places the adaptive filters between the back-EMF estimator and quadrature PLL. Unlike low-pass filters (LPFs), these adaptive filters can extract the desired component without magnitude and phase loss, which will be more feasible in back-EMF filtering. The adaptive filters have been widely investigated in [26] and [27] and can be roughly grouped into resonant filter and digital filter. The resonant filter, such as second-order generalized integrator (SOGI) [26] and adaptive vectorial filter, [27] is proposed to extract fundamental component from distorted signal. However, these methods are unable to compensate the harmonics completely and an additional frequency-locked loop is needed to ensure its tracking performance. Digital filters, based on delay operator or adaptive noise cancellation, have been designed for harmonic elimination to achieve high control performance. In [28] and [29], the digital filter based on delay operator is proposed to eliminate harmonic influence, but these methods may face sharp phase jump and lead to spurious transient, since it highly relies on the periodicity of the estimated signal. Another digital filter based on adaptive noise cancellation is capable to compute the desired signal by self-adjusting harmonic coefficients according to the signal attribute and operating environment. The digital filters based on least square adaptive filter [30] and recursive least mean square adaptive filter [19] are proposed for fundamental back-EMF extraction and realize the low-order harmonics elimination accurately by updating filter coefficients online. However, both of them require a heavy calculation burden and are hard to implement. In view of this shortcoming, the two-sample-based algorithm, avoiding the external reference signal injection, is put forward to relieve the calculation burden [31], but its bandwidth is fixed and not feasible for frequency variation condition.

In this article, a newly adaptive training control-based filter, inserted between the SMO and PLL, is proposed for precise position estimation in sensorless control of IPMSM, eliminating the harmonics by using the steepest-descent algorithm, which has a simpler structure and less computation burden since its reference signal is self-generated. Meanwhile, the proposed method has enough degree of freedom, which is capable to tune the bandwidth to satisfy the demands of different frequency scenarios. The rest of this article is organized as follows. Section II analyzes the causes of sixth position harmonic ripple in detail. In Section III, based on adaptive noise cancellation, the proposed filter is designed and self-tuned by searching for minimal value of designed objective function. The experimental verifications are shown in Section IV. Finally, Section V concludes the article.

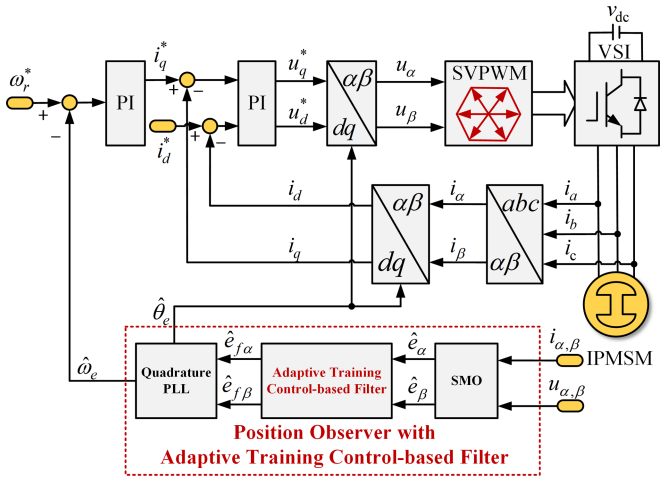

Fig. 1. Block diagram of sensorless control system based on back-EMF model.

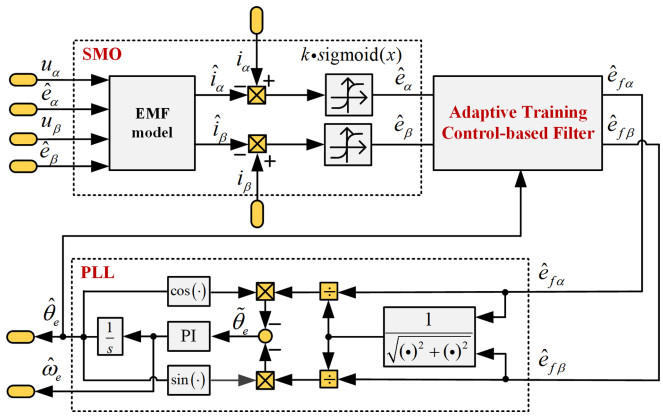

Fig. 2. Position observer with adaptive training control-based filter.

II. Sensorless Control Scheme of Rotor Position for IPMSM

A. Back-EMF Model-Based Sensorless Control

An overview of the proposed sensorless control system on the basis of back-EMF model is presented in Fig. 1, where a position observer embedding with adaptive training control-based filter in Fig. 2 is utilized to extract fundamental components in the back-EMF.

The IPMSM voltage equation in the $\alpha\beta$ reference frame can be given as

$$\begin{bmatrix} u_\alpha \\ u_\beta \end{bmatrix} = \begin{bmatrix} R_s + pL_q & 0 \\ 0 & R_s + pL_q \end{bmatrix} \begin{bmatrix} i_\alpha \\ i_\beta \end{bmatrix} + \begin{bmatrix} e_\alpha \\ e_\beta \end{bmatrix} \tag{1}$$

where u_α and u_β represent α-axis and β-axis stator voltages, i_α and i_β represent α-axis and β-axis stator currents. L_q denotes the q-axis inductances; R_s is the stator resistance; ω_e is the electrical speed, $p = d/dt$ is the differential operator. e_α and e_β are equivalent back-EMFs, which can be expressed as

$$\begin{bmatrix} e_\alpha \\ e_\beta \end{bmatrix} = [\lambda_f + (L_d - L_q) i_d] \omega_e \begin{bmatrix} -\sin\theta_e \\ \cos\theta_e \end{bmatrix} \tag{2}$$

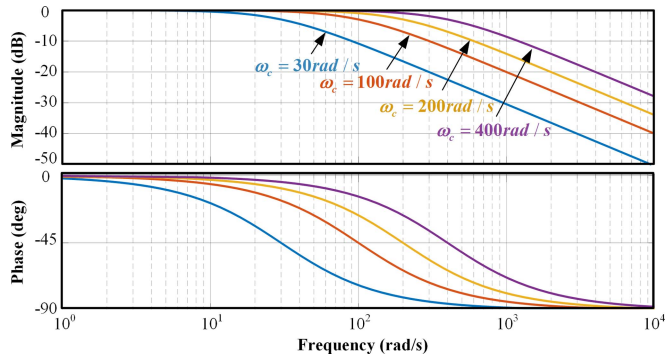

Fig. 3. Bode diagram of LPF with different ω_c.

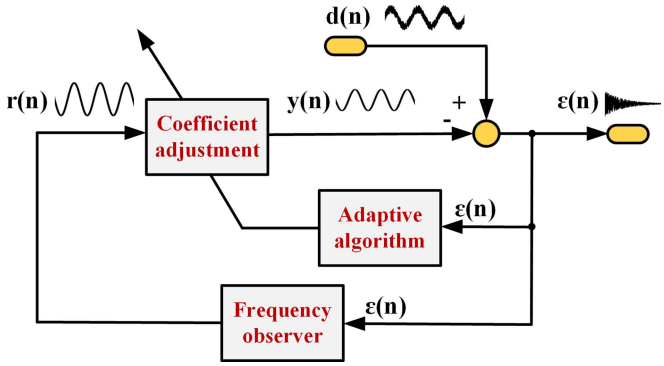

Fig. 4. Working principle of adaptive noise-cancellation.

where λ_f is the rotor magnet flux, $\lambda_a = \lambda_f + (L_d - L_q)i_d$ is the active flux, θ_e is the rotor electrical position.

Then, a back-EMF model-based SMO for estimating the rotor position can be described as

$$\frac{d}{dt}\begin{bmatrix}\hat{i}_\alpha \\ \hat{i}_\beta\end{bmatrix} = \frac{1}{L_q}\begin{bmatrix}u_\alpha \\ u_\beta\end{bmatrix} - \frac{R_s}{L_q}\begin{bmatrix}\hat{i}_\alpha \\ \hat{i}_\beta\end{bmatrix} - \frac{1}{L_q}\begin{bmatrix}k_{\text{SMO}}H\left(\hat{i}_\alpha - i_\alpha\right) \\ k_{\text{SMO}}H\left(\hat{i}_\beta - i_\beta\right)\end{bmatrix} \tag{3}$$

where "^" denotes the estimated value. k_{SMO} is the gain of SMO, and H denotes the sigmoid function, which can be expressed as

$$\begin{bmatrix}H\left(\tilde{i}_\alpha\right) \\ H\left(\tilde{i}_\beta\right)\end{bmatrix} = \begin{bmatrix}\left(\frac{2}{1+\exp\left(-a\tilde{i}_\alpha\right)}\right) - 1 \\ \left(\frac{2}{1+\exp\left(-a\tilde{i}_\beta\right)}\right) - 1\end{bmatrix} \tag{4}$$

where $a > 0$ denotes the slope of function, $\tilde{i}_{\alpha,\beta} = \hat{i}_{\alpha,\beta} - i_{\alpha,\beta}$ denote stator current estimation errors. The fundamental components of estimated back-EMF $\hat{e}_{f\alpha,\beta}$ can be obtained through LPFs, which can be described as

$$\begin{bmatrix}\hat{e}_{f\alpha} \\ \hat{e}_{f\beta}\end{bmatrix} = \frac{\omega_c}{s+\omega_c}\begin{bmatrix}\hat{e}_\alpha \\ \hat{e}_\beta\end{bmatrix} \tag{5}$$

where ω_c represents the cutoff frequency of the LPFs.

It can be found in (5) that the LPFs applied in SMO have the characteristic of suppressing high-order harmonics to reduce the chattering phenomenon. However, the phase lag is introduced in the back-EMF estimates due to the property of the LPFs. Fig. 3 demonstrates the harmonic rejection and phase lag. A smaller ω_c exhibits better harmonic suppression performance but introduces a larger phase delay.

B. Effects of Harmonics on Quadrature PLL

The estimated back-EMF is contaminated with $\pm(6k \pm 1)$ harmonics since the stator currents are distorted by the inverter nonlinearity and flux spatial harmonics. Therefore, the back-EMF estimations are described as

$$\begin{bmatrix}\hat{e}_\alpha \\ \hat{e}_\beta\end{bmatrix} = \begin{bmatrix}\hat{e}_{f\alpha} + \hat{e}_{h\alpha} \\ \hat{e}_{f\beta} + \hat{e}_{h\beta}\end{bmatrix} \tag{6}$$

where $\hat{e}_{f\alpha,\beta}$ are the back-EMF fundamental components estimates, and $\hat{e}_{h\alpha,\beta}$ are the harmonics and can be given by

$$\begin{bmatrix}\hat{e}_{h\alpha} \\ \hat{e}_{h\beta}\end{bmatrix} = \begin{bmatrix}-e_{6k-1}\sin(-(6k-1)\omega_e t + \varphi_{6k-1}) \\ e_{6k-1}\cos(-(6k-1)\omega_e t + \varphi_{6k-1})\end{bmatrix} + \begin{bmatrix}-e_{6k+1}\sin((6k+1)\omega_e t + \varphi_{6k+1}) \\ e_{6k+1}\cos((6k+1)\omega_e t + \varphi_{6k+1})\end{bmatrix} \tag{7}$$

where $\hat{e}_{6k-1}$, $\hat{e}_{6k+1}$, φ_{6k-1}, and φ_{6k+1} denote the amplitudes and the initial phase of the $(6k-1)$th and $(6k+1)$th harmonic, respectively.

When the equivalent back-EMFs are observed, the position error $\tilde{\theta}_e$ obtained by PLL can be written as

$$\begin{aligned}\tilde{\theta}_e &= \frac{1}{\sqrt{\hat{e}_\alpha^2 + \hat{e}_\beta^2}}\left(-\hat{e}_\alpha\cos\hat{\theta}_e - \hat{e}_\beta\sin\hat{\theta}_e\right) \\ &\approx \theta_e - \hat{\theta}_e \pm \frac{1}{\sqrt{\hat{e}_\alpha^2 + \hat{e}_\beta^2}}e_{6k}\sin\left(6k\hat{\omega}_e t + \varphi_{6k}\right)\end{aligned} \tag{8}$$

where e_{6k} and φ_{6k} represent the amplitude and the initial phase angle of the $6k$th equivalent back-EMF harmonics.

As can be seen in (8), both dc-bias and $6k$th harmonics contained in signal $\tilde{\theta}_e$, which display as an additional error (especially the $6k$th harmonic fluctuations), reducing the rotor position estimation accuracy.

III. Adaptive Training Control-Based Filter

An appropriate cutoff frequency for LPFs is troublesome to completely eliminate the harmonics without influencing the fundamental back-EMF. Therefore, according to the Wiener theory [31], the adaptive noise-cancelling principle has been proposed, which is a promising method to track the specific harmonic by self-updating the filter coefficients.

A. Principle of Proposed Adaptive Filter

Fig. 4 shows the working principle of adaptive noise cancellation. $d(n)$ denotes the original input signal contaminated by harmonics. The reference signal $r(n)$ processed by frequency observer is highly relevant to the desired signal. The output signal $y(n)$ can track the desired signal accurately through iterative calculation according to the adaptive algorithm.

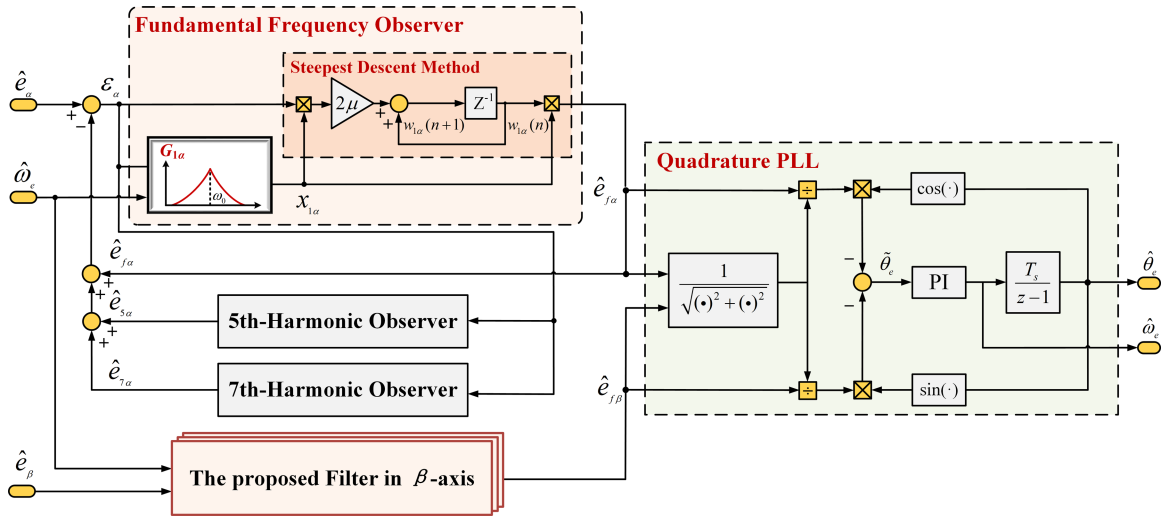

Fig. 5. Block diagram of adaptive training control-based filter.

Considering the distortion of the back-EMF mainly contained with the fifth and seventh harmonics, a three-layer filter based on the adaptive noise-cancellation principle is proposed to extract the fundamental components $\hat{e}_{f\alpha,\beta}$. For convenient analysis, Fig. 5 shows the specific structure of the adaptive filter in the α-axis.

The estimated back-EMF $\hat{e}_\alpha$ is composed of the fundamental components $\hat{e}_{f\alpha}$, fifth and seventh components ($\hat{e}_{5\alpha}$ and $\hat{e}_{7\alpha}$), corresponding to $d(n)$ in Fig. 4. The estimated speed $\hat{\omega}_e$ is provided by the quadrature PLL multiplying with respective order to provide resonant frequency for frequency observer to generate the reference signal $x_{i\alpha}(n)$, where subscript $i = 15{,}7$ is the respective order of the adaptive filter at the fundamental and harmonic frequencies. As shown in Fig. 5, the desired signal $\hat{e}_{f\alpha}$ is acquired through the error signal $\varepsilon_\alpha(n)$ by subtracting $\hat{e}_{5\alpha}$ and $\hat{e}_{7\alpha}$ from $\hat{e}_\alpha$. The coefficients $w_{i\alpha}(n)$ can be updated by the steepest descent algorithm to achieve convergence once each estimate $w_{i\alpha}x_{i\alpha}(n)$ tracks the actual value of fundamental component and harmonics.

B. Design of Frequency Observer

It is noted that unlike the conventional adaptive filter, the reference signal of the proposed filter is not needed for external injection, it only requires to extract the corresponding frequency components in the error signal through the module $G_{i\alpha}$. As illustrated in Fig. 5, the transfer function from input signal $\hat{e}_\alpha$ to error signal ε_α can be deduced as

$$\frac{\varepsilon_\alpha(z)}{\hat{e}_\alpha(z)} = \frac{1}{1+\sum_{i=1,5,7} H_i(z)} \tag{9}$$

where the frequency observer $H_i(z)$ is comprised of module $G_{i\alpha}$ and the coefficient adjustment via a steepest descent algorithm. Therefore, $G_{i\alpha}$ should be designed to guarantee its characteristic of high gain without phase deviation, so the output signal of every layer has the same phase as the desired signal at the corresponding frequency. Inspired by the resonant controller, the transfer function of $G_{i\alpha}$ can be given as

$$G_{i\alpha}(z) = Z\left(\frac{k\omega_0 s}{s^2+\omega_0^2}\right)\Big|_{s=\frac{2}{T_s}\frac{z-1}{z+1}} \tag{10}$$

where k is the resonance gain, T_s is the sampling period, and ω_0 denotes the resonant angular frequency. From previous research [32], the amplitude-frequency response of the module $G_{i\alpha}$ is infinite at ω_0. Take the fundamental frequency component for example, its output signal $x_{\alpha 1}(n)$ is the sample sinusoid sequence processed by the frequency observer, which can be expressed as

$$x_\alpha(n) = C\cos(n\hat{\omega}_e T_s + \phi) \tag{11}$$

where C represents the amplitude of the sinusoid sequence at the specified $\hat{\omega}_e$, the phase ϕ is the same as the desired output signal.

C. Adjustment of Coefficients

From the block diagram in Fig. 5, the instantaneous error of the filter is

$$\varepsilon_\alpha(n) = \hat{e}_\alpha(n) - \sum_{i=\{1,5,7\}} w_{i\alpha}(n)x_{i\alpha}(n). \tag{12}$$

$J(n)$ can be equal to the half of the squared-error criterion function, which is a widely used objective function. The vector format of $J(n)$ can be shown as

$$J(n) = \frac{1}{2}\varepsilon_\alpha(n)^2 = \frac{1}{2}(\hat{e}_\alpha(n) - W_\alpha(n)X_\alpha(n))^2 \tag{13}$$

where the vector $X_a(n)$ and coefficient vector $W_a(n)$ at sample point n can be presented as

$$\begin{aligned} X_\alpha(n) &= [x_{1\alpha}(n)x_{5\alpha}(n)x_{7\alpha}(n)] \\ W_\alpha(n) &= [w_{1\alpha}(n)w_{5\alpha}(n)w_{7\alpha}(n)]. \end{aligned} \tag{14}$$

From (13), $W_a(n)$ can be updated to minimize the objective function $J(n)$ according to the steepest descent algorithm along

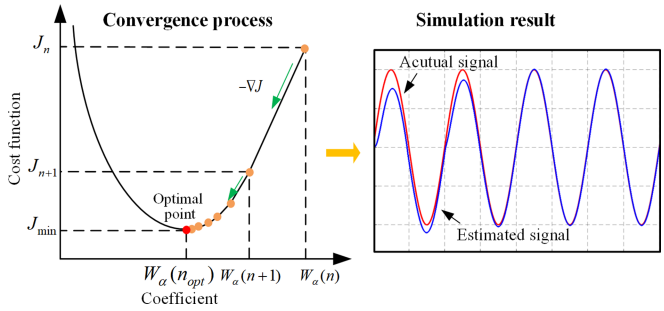

Fig. 6. Basic principle of the steepest descent method in adaptive filter.

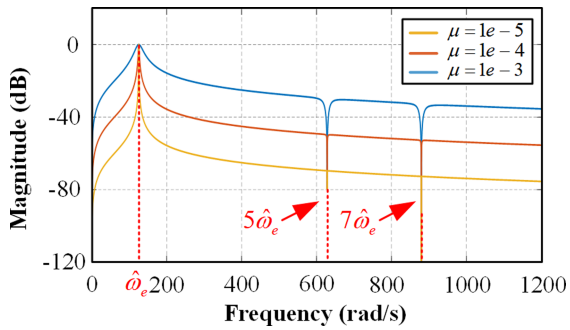

Fig. 7. Frequency response of $F(z)$ with different μ, where $\hat{\omega}_e = 2\pi \cdot 20$ rad/s.

the negative gradient. The opposite gradient of $J(n)$ is related to $W_a(n)$, represented by $-\nabla J(n)$, which can be written as

$$-\nabla J(n) = \left(\hat{e}_\alpha(n) - W_\alpha(n) X_\alpha^T(n)\right) X_\alpha(n) = \varepsilon_\alpha(n) X_\alpha(n). \quad (15)$$

It is clear that the coefficients vector adjustment rule can be given as [29]

$$W_\alpha(n+1) = W_\alpha(n) + \mu\varepsilon_\alpha(n) X_\alpha(n) \quad (16)$$

where μ is the learning rate. The basic principle of the steepest descent algorithm in the proposed filter, as shown in Fig. 6, graphically presents the objective function $J(n)$ related to the coefficient vector $W_a(n)$. It can be seen that as the coefficient vector moves toward the opposite direction of the $\nabla J(n)$, the objective function $J(n)$ approaches the optimal point after multiple iterations, which reflects the estimated signal converges to the actual one.

Hence, the open loop transfer function from $\varepsilon_\alpha(z)$ to $\hat{e}_{f\alpha}(z)$ can be described as

$$H_1(z) = \frac{\hat{e}_{f\alpha}(z)}{\varepsilon_\alpha(z)} = \frac{2\mu C^2(z\cos\omega_0 T_s - 1)}{z^2 - 2z\cos\omega_0 T_s + 1}. \quad (17)$$

In the case of the proposed filter with three-layer, the transfer function of the proposed method can be expressed as

$$F(z) = \frac{H_1(z)}{1 + \sum_{i=1,5,7} H_i(z)}. \quad (18)$$

Fig. 7 shows the frequency response of $F(z)$ with different learning rate μ. It is clear that the bandwidth of the proposed filter is highly dependent on the μ. The different values of μ could affect the convergence rate and the harmonics suppression accuracy. A smaller μ represents a high harmonic-filtering capability, which may cause a larger convergence time. Therefore, an appropriate value of μ should be chosen carefully to obtain a tradeoff between the convergence rate and the steady-state error in estimating the fundamental components $\hat{e}_{f\alpha}$.

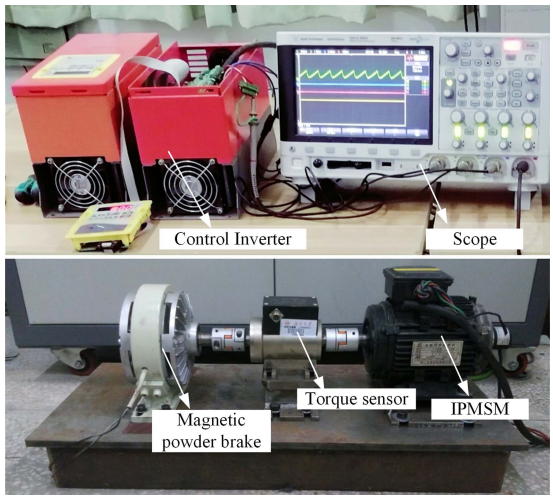

Fig. 8. Experimental platform for 1.5 kW sensorless IPMSM drive.

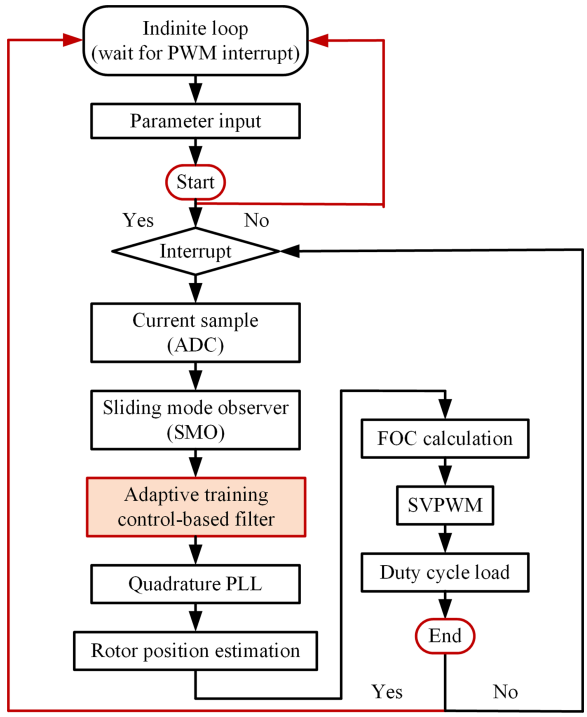

Fig. 9. Software flow chart of IPMSM based on adaptive training control-based filter.

IV. Experimental Results

The proposed sensorless control method based on the adaptive training control-based filter has been verified on the experimental platform, as shown in Fig. 8. The rated IPMSM

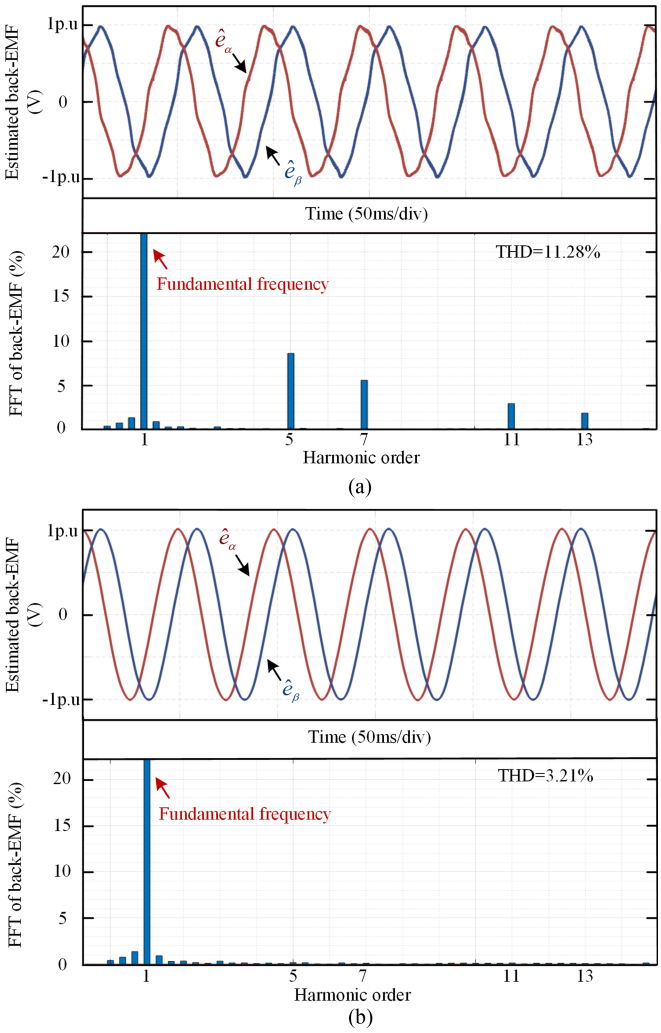

Fig. 10. Back-EMF estimations and corresponding FFT analysis at 600 r/min under 50% rated load. (a) Adaptive training control-based filter disabled. (b) Adaptive training control-based filter enabled.

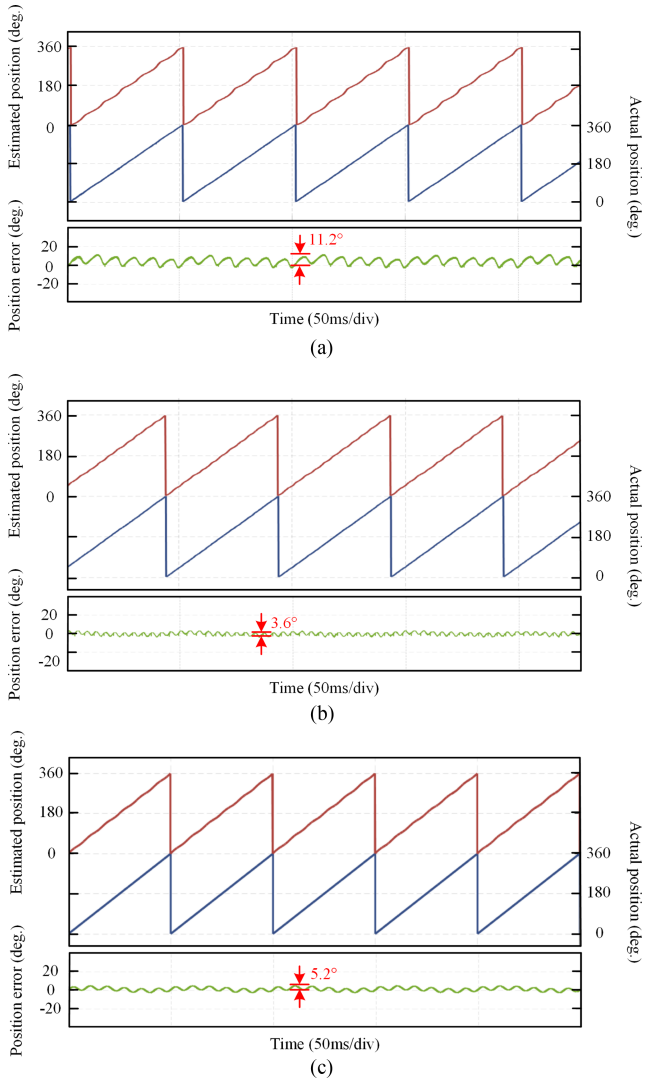

Fig. 11. Estimated rotor position at 600 r/min under 50% rated load. (a) Adaptive training control-based filter disabled. (b) Adaptive training control-based filter enabled. (c) SOGI enabled.

TABLE I
EXPERIMENT IPMSM PARAMETERS

Parameters	Values	Parameters	Values
Rated power /kW	1.5	Rated torque/N.m	9.4
Rated voltage /V	380	Number of pole pairs	2
Rated current /A	2.7	D-axis inductance/mH	37.78
Rated speed /(r/min)	1500	Q-axis inductance/mH	119.62
Stator resistance / Ω	3.678	Rotor flux linkage /Wb	0.803

parameters are listed in Table I. The load torque is provided by a magnetic powder brake connected with the test IPMSM. An incremental encoder (PENON-K3808G) is used for rotor position information acquisition, which is for comparison only. The experiment was implemented by a DSP TMS320F2808 and the control frequency was 10 kHz. The software flow chart of IPMSM based on the adaptive training control-based filter is illustrated in Fig. 9.

The back-EMF estimation waveforms and their FFT analysis before and after applying the adaptive training control-based filter in the steady state are presented in Fig. 10. From Fig. 10(a), the −5th, 7th, −11th, and 13th harmonic components can be seen obviously without the proposed method, where the −5th and 7th harmonics take up relatively large shares. However, Fig. 10(b) shows that principal harmonics are significantly attenuated and the waveform of the estimated back-EMF becomes more sinusoidal after applying the proposed method, where the THD decreases by 8.07%.

For the purpose of investigating the control performance in the steady state, the experimental comparison of the position estimation under the 50% rated load is illustrated in Fig. 11. As can be observed in Fig. 11(a), the rotor position estimation is polluted with an obvious 6th harmonic ripple due to back-EMF estimates distortion, and the maximum value of the rotor position error reaches up to 11.2°. On the contrary, it is clear in Fig. 11(b) that the estimated position is almost the same as the real one and the position error decreases to 3.6° after applying the proposed method. As a consequence, the position estimation performance of the proposed method is verified. Furthermore,

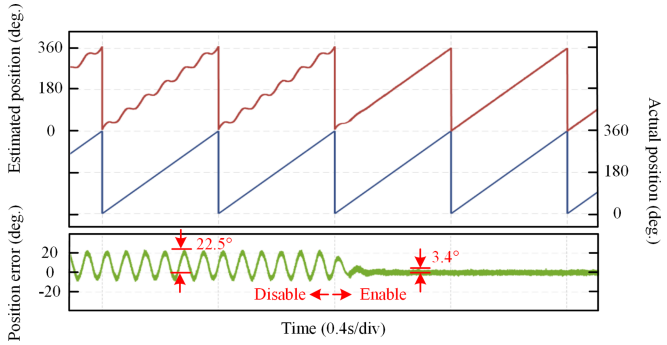

Fig. 12. Experimental results of rotor position estimation at 75 r/min under 50% rated load.

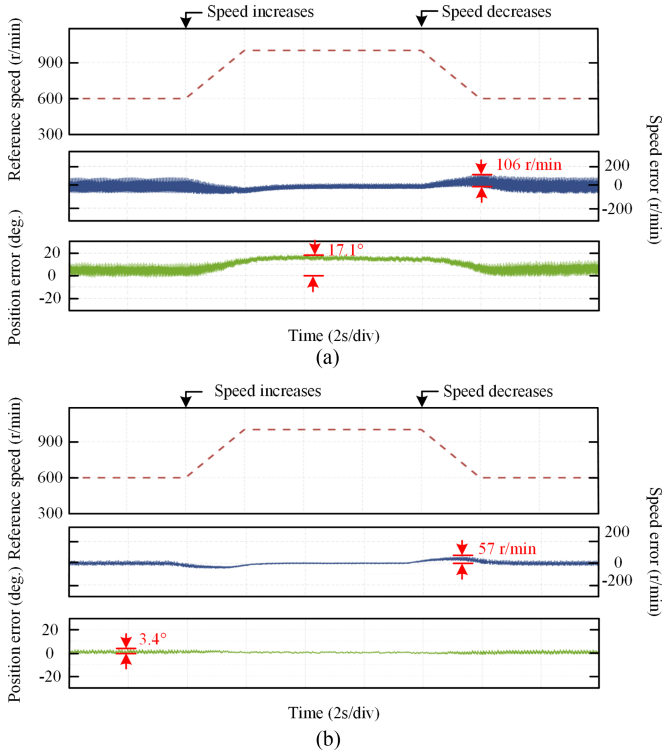

Fig. 13. Estimated speed and position errors under 50% rated load from 600 to 1000 r/min. (a) Adaptive training control-based filter disabled. (b) Adaptive training control-based filter enabled.

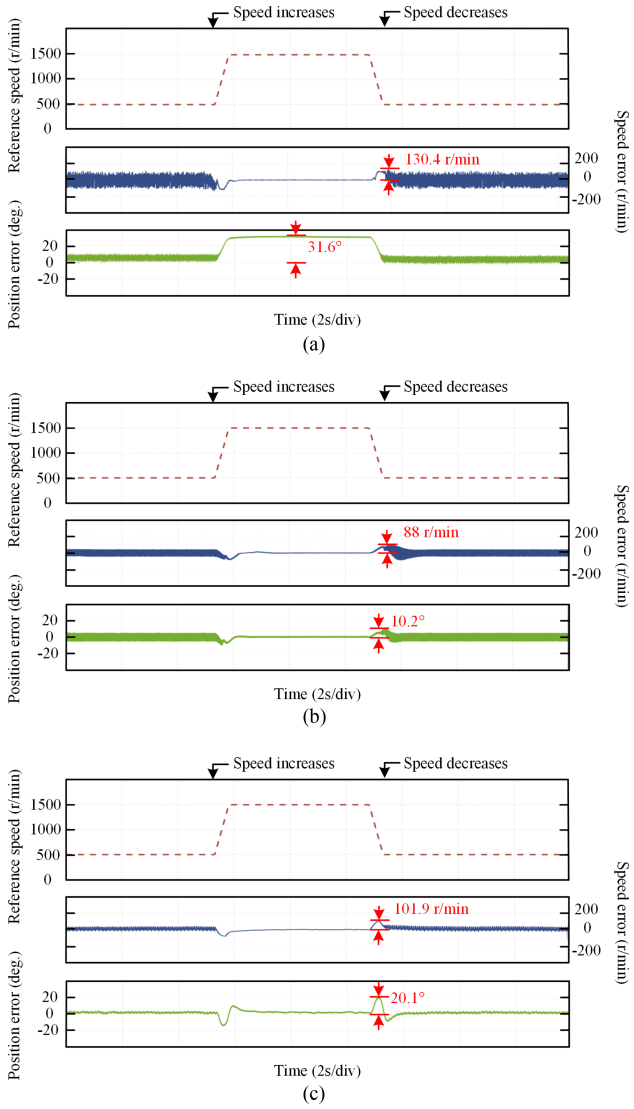

Fig. 14. Estimated speed and position errors under 50% rated load for fast acceleration and deceleration. (a) Adaptive training control-based filter disabled. (b) SOGI enabled. (c) Adaptive training control-based filter enabled.

Fig. 11(c) reveals that the adaptive training control-based filter has lower rotor position error compared to the SOGI.

On the other hand, as shown in Fig. 12, when IPMSM rotates at 75 r/min under 50% rated load, the signal-to-noise ratio of the back-EMF estimations is reduced as the motor velocity decelerates, the rotor position error reaches 22.5° before the proposed method enabled. However, the sixth position harmonic ripple is suppressed after the proposed method is enabled, which means the adaptive training control-based filter could work actively in the low-speed domain.

The control behavior of the proposed method in the speed transient state is validated. The rotor position error, depicted in Fig. 13(a), contains distinct fluctuations without the proposed method. Instead, the rotor position error is visibly decreased as the proposed method is applied. In Fig. 13(b), the maximal position and speed errors are 3.4°/57 r/min. The experimental result shows excellent distortion rejection and accurate position estimation performance of the proposed method.

Additionally, Fig. 14 compares the experimental results in a more rapid speed acceleration and deceleration, from 500 to 1500 r/min in 0.5 s (ramp slope is 2000 r/min/s). Fig. 14 reveals that the position and speed estimation in both methods deviates more dramatically compared to the low-speed ramp slope. Meanwhile, the maximum position/speed error in the proposed method is 20.1°/101.9 r/min, which means the proposed method could track the rotor position and speed under high-speed ramp slope, even though the estimation error is higher than SOGI.

The experimental results of position and speed error with and without the proposed method under multispeed operation with rated load are shown in Fig. 15. The speed changes from 300 to 1500 r/min, increasing 300 r/min in order. From Fig. 15(a), when

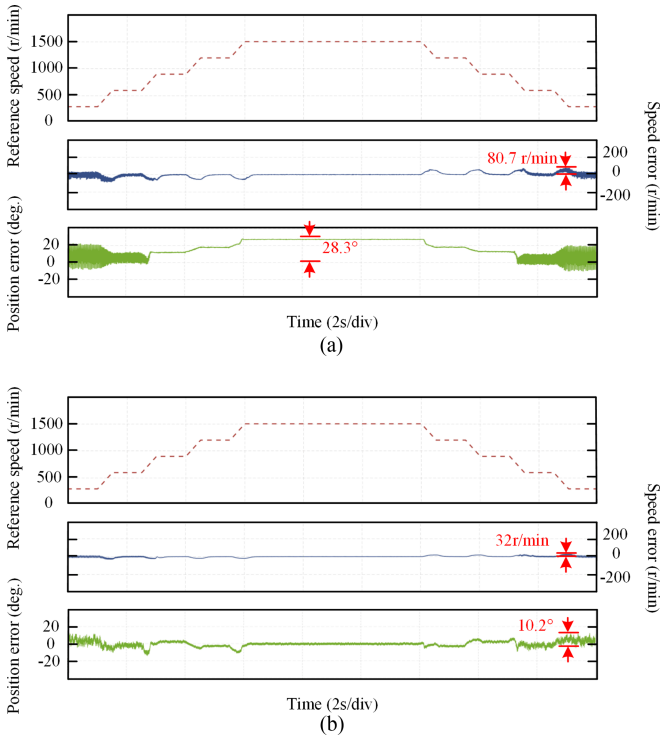

Fig. 15. Estimated speed and position errors with rated load under multispeed operation. (a) Adaptive training control-based filter disabled. (b) Adaptive training control-based filter enabled.

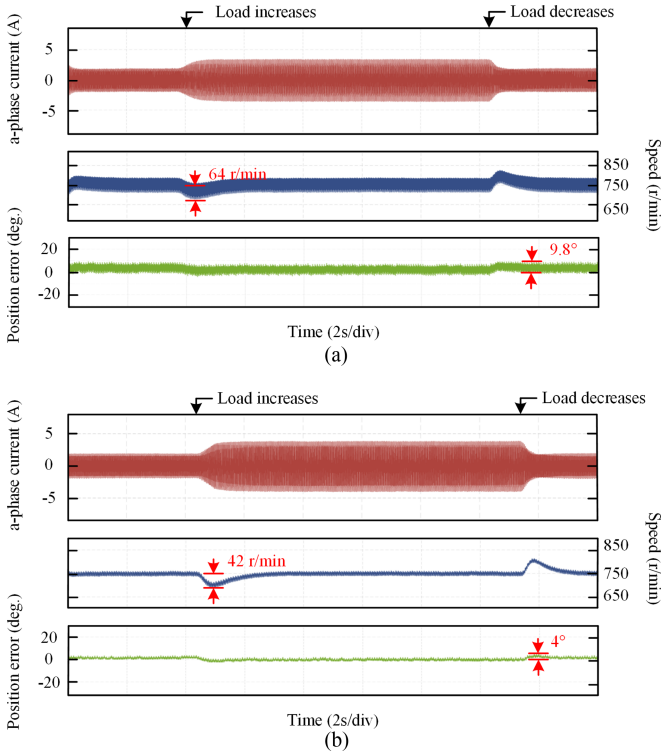

Fig. 16. Estimated speed and position errors at 750 r/min from 50% to 100% rated load. (a) Adaptive training control-based filter disabled. (b) Adaptive training control-based filter enabled.

the proposed method is disabled, the position error gets larger as the motor velocity increases, which cannot meet the estimation requirement. For comparison, after using the proposed method, the position and speed error are restricted within a tolerable range. Therefore, the proposed adaptive training control-based filter has a better estimation performance at different speeds.

Furthermore, for validating the control performance of the proposed method in a load transient state, with load changing from 50% to 100% of the rated torque at 750 r/min, as shown in Fig. 16. In Fig. 16(a), the position error without the proposed filter is notable under different situations. In contrast, the proposed method could remove these undesired components and perform better during the entire operation. It is revealed that the transient position errors are within 4°, which is considerably lower than the case without measures. Obviously, the speed deviation under the step-load is also lower, which implies the proposed method is robust under the speed control condition in sensorless IPMSM drives under distorted conditions.

Additionally, the experiments under rated speed with different loads are conducted, as presented in Fig. 17. The load command changes from 0% to 100% rated load, increasing 20% rated load in order. It is observed in Fig. 17(a) that the position/speed error without using the proposed method is 12.4° / 54 r/min. However, after using the proposed method in Fig. 17(b), the position/speed error is decreased to 7.5° / 15.2 r/min. These results verify that the proposed adaptive training control-based filter has an excellent control performance at different loads condition.

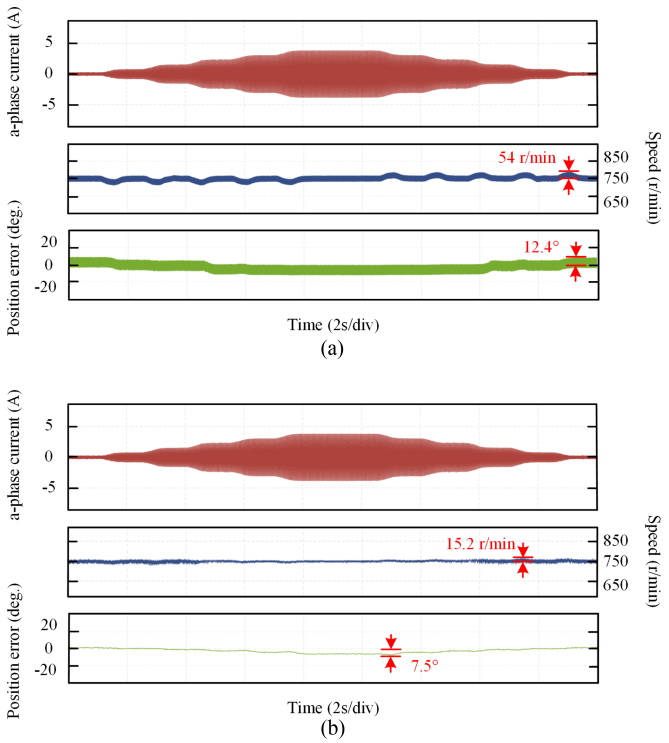

Fig. 17. Estimated speed and position errors at 1500 r/min with multiload operation. (a) Adaptive training control-based filter disabled. (b) Adaptive training control-based filter enabled.

V. Conclusion

To increase the accuracy of position estimation, an adaptive training control-based filter combined with an SMO is presented in this article to realize precise position estimation. This method, based on the steepest descent algorithm, is capable of self-adjusting harmonic coefficients to filter out the harmonics of estimated back-EMF. Moreover, the proposed adaptive filter requires less calculation burden, since its reference signal is self-generated without external injection. The experiments demonstrated a 1.5-kW IPMSM sensorless drive to verify the feasibility of the proposed sensorless method. The experimental results show that the proposed method can diminish the fifth and seventh harmonics contained in the back-EMF estimates remarkably. The dynamic performance of the proposed method in the speed transient state and load transient state are also improved by intensive experimental comparison. Consequently, the proposed adaptive training control-based filter is an effective method to enhance the sensorless IPMSM control performance.

References

[1] X. Wu et al., "Hybrid position estimation strategy with a smooth transition for IPMSM sensorless drives in the wide speed range," *IEEE Trans. Power Electron.*, vol. 37, no. 7, pp. 7916–7927, Jul. 2022.

[2] W. Xu, Y. Jiang, C. Mu, and F. Blaabjerg, "Improved nonlinear flux observer-based second-order SOIFO for PMSM sensorless control," *IEEE Trans. Power Electron.*, vol. 34, no. 1, pp. 565–579, Jan. 2019.

[3] D. F. Alonso, Y. Kang, D. Fernández Laborda, M. M. Gómez, D. D. Reigosa, and F. Briz, "Permanent magnet synchronous machine torque estimation using low cost hall-effect sensors," *IEEE Trans. Ind. Appl.*, vol. 57, no. 4, pp. 3735–3743, Jul./Aug. 2021.

[4] G. Pellegrino, A. Vagati, P. Guglielmi, and B. Boazzo, "Performance comparison between surface-mounted and interior PM motor drives for electric vehicle application," *IEEE Trans. Ind. Electron.*, vol. 59, no. 2, pp. 803–811, Feb. 2012.

[5] L. Yan et al., "Suppression of major current harmonics for dual three-phase PMSMs by virtual multi three-phase systems," *IEEE Trans. Ind. Electron.*, vol. 69, no. 6, pp. 5478–5490, Jun. 2022.

[6] I. Boldea, M. C. Paicu, and G.-D. Andreescu, "Active flux concept for motion-sensorless unified AC drives," *IEEE Trans. Power Electron.*, vol. 23, no. 5, pp. 2612–2618, Sep. 2008.

[7] Z. Chen, J. Qiu, and M. Jin, "Prediction-error-driven position estimation method for finite-control-set model predictive control of interior permanent-magnet synchronous motors," *IEEE J. Emerg. Topic Power Elect.*, vol. 7, no. 1, pp. 282–295, Mar. 2019.

[8] H. Zhang, W. Liu, Z. Chen, and N. Jiao, "Smooth transition of multimode synchronous modulation for IPMSM sensorless drives in rail-transit applications," *IEEE Trans. Ind. Electron.*, vol. 68, no. 1, pp. 128–138, Jan. 2021.

[9] S.-I. Kim, J.-H. Im, E.-Y. Song, and R.-Y. Kim, "A new rotor position estimation method of IPMSM using all-pass filter on high-frequency rotating voltage signal injection," *IEEE Trans. Ind. Electron.*, vol. 63, no. 10, pp. 6499–6509, Oct. 2016.

[10] J. Wei, H. Lu, H. Xue, Z. Zhang, and B. Zhou, "The rotor position estimation error improved method for sensorless starting control of brushless synchronous machine," *IEEE Trans. Power Electron.*, vol. 35, no. 8, pp. 8384–8395, Aug. 2020.

[11] J. Holtz, "Acquisition of position error and magnet polarity for sensorless control of PM synchronous machines," *IEEE Trans. Ind. Appl.*, vol. 44, no. 4, pp. 1172–1180, Jul/Aug. 2008.

[12] M. E. Haque, L. Zhong, and M. F. Rahman, "A sensorless initial rotor position estimation scheme for a direct torque controlled interior permanent magnet synchronous motor drive," *IEEE Trans. Power Electron.*, vol. 18, no. 6, pp. 1376–1383, Nov. 2003.

[13] J. Lara and A. Chandra, "Performance investigation of two novel HSFSI demodulation algorithms for encoderless FOC of PMSMs intended for EV propulsion," *IEEE Trans. Ind. Electron.*, vol. 65, no. 2, pp. 1074–1083, Feb. 2018.

[14] C.-Y. Yu, J. Tamura, D. D. Reigosa, and R. D. Lorenz, "Position self-sensing evaluation of a FI-IPMSM based on high-frequency signal injection methods," *IEEE Trans. Ind. Electron.*, vol. 49, no. 2, pp. 880–888, Mar./Apr. 2013.

[15] X. Song, B. Han, S. Zheng, and S. Chen, "A novel sensorless rotor position detection method for high-speed surface PM motors in a wide speed range," *IEEE Trans. Power Electron.*, vol. 33, no. 8, pp. 7083–7093, Aug. 2018.

[16] Z. Yin, Y. Zhang, X. Cao, D. Yuan, and J. Liu, "Estimated position error suppression using novel PLL for IPMSM sensorless drives based on full-order SMO," *IEEE Trans. Power Electron.*, vol. 37, no. 4, pp. 4463–4474, Apr. 2022.

[17] S.-C. Yang and G.-R. Chen, "High-speed position-sensorless drive of permanent-magnet machine using discrete-time EMF estimation," *IEEE Trans. Ind. Electron.*, vol. 64, no. 6, pp. 4444–4453, Jun. 2017.

[18] D. Xiao, S. Nalakath, Y. Sun, J. Wiseman, and A. Emadi, "Complex-coefficient adaptive disturbance observer for position estimation of IPMSMs with robustness to DC errors," *IEEE Trans. Ind. Electron.*, vol. 67, no. 7, pp. 5924–5935, Jul. 2020.

[19] G. Wang, T. Li, G. Zhang, X. Gui, and D. Xu, "Position estimation error reduction using recursive-least-square adaptive filter for model-based sensorless interior permanent-magnet synchronous motor drives," *IEEE Trans. Ind. Electron.*, vol. 61, no. 9, pp. 5115–5125, Sep. 2014.

[20] X. Wu et al., "Enhanced position sensorless control using bilinear recursive least squares adaptive filter for interior permanent magnet synchronous motor," *IEEE Trans. Power Electron.*, vol. 35, no. 1, pp. 681–698, Jan. 2020.

[21] Y. Park and S.-K. Sul, "A novel method utilizing trapezoidal voltage to compensate for inverter nonlinearity," *IEEE Trans. Power Electron.*, vol. 27, no. 12, pp. 4837–4846, Dec. 2012.

[22] Y. Inoue, K. Yamada, S. Morimoto, and M. Sanada, "Effectiveness of voltage error compensation and parameter identification for model-based sensorless control of IPMSM," *IEEE Trans. Ind. Appl.*, vol. 45, no. 1, pp. 213–221, Jan./Feb. 2009.

[23] R. W. Hejny and R. D. Lorenz, "Evaluating the practical low-speed limits for back-EMF tracking-based sensorless speed control using drive stiffness as a key metric," *IEEE Trans. Ind. Appl.*, vol. 47, no. 3, pp. 1337–1343, May/Jun. 2011.

[24] S.-Y. Kim, W. Lee, M.-S. Rho, and S.-Y. Park, "Effective dead-time compensation using a simple vectorial disturbance estimator in PMSM drives," *IEEE Trans. Ind. Electron.*, vol. 57, no. 5, pp. 1609–1614, May 2010.

[25] S.-H. Jung, H. Kobayashi, S. Doki, and S. Okuma, "An improvement of sensorless control performance by a mathematical modelling method of spatial harmonics for a SynRM," *Proc. Power Electron. Conf.*, 2020, pp. 2010–2015.

[26] F. U. Nazir, N. Kumar, B. C. Pal, B. Singh, and B. K. Panigrahi, "Enhanced SOGI controller for weak grid integrated solar PV system," *IEEE Trans. Energy Convers.*, vol. 35, no. 3, pp. 1208–1217, Sep. 2020.

[27] S. Vazquez, J. A. Sanchez, M. R. Reyes, J. I. Leon, and J. M. Carrasco, "Adaptive vectorial filter for grid synchronization of power converters under unbalanced and/or distorted grid conditions," *IEEE Trans.Ind. Electron.*, vol. 61, no. 3, pp. 1355–1367, Mar. 2014.

[28] D. Xiao et al., "Computation-efficient position estimation algorithm for permanent magnet synchronous motor drives under distorted conditions," *IEEE J. Emerg. Sel. Topics Power Electron.*, vol. 9, no. 3, pp. 2759–2773, Jun. 2021.

[29] H. Wang et al., "A delay-based frequency estimation scheme for speed-sensorless control of induction motors," *IEEE Trans. Ind. Appl.*, vol. 58, no. 2, pp. 2107–2121, Mar./Apr. 2022.

[30] G. Wang, H. Zhan, G. Zhang, X. Gui, and D. Xu, "Adaptive compensation method of position estimation harmonic error for EMF-based observer in sensorless IPMSM drives," *IEEE Trans. Power Electron.*, vol. 29, no. 6, pp. 3055–3064, Jun. 2014.

[31] P. Lamo, A. Pigazo, and F. J. Azcondo, "Two-sample PLL with harmonic filtering capability applicable to single-phase grid-connected converters," *IEEE J. Emerg. Sel. Topics Power Electron.*, vol. 9, no. 3, pp. 3072–3082, Jun. 2021.

[32] F. Boroujeny, *Adaptive Filters: Theory and Applications*. Hoboken, NJ, USA: Wiley, 2013.

[33] W.-K. Sou, C.-W. Chao, C. Gong, C.-S. Lam, and C.-K. Wong, "Analysis, design, and implementation of multi-quasi-proportional-resonant controller for thyristor-controlled LC-coupling hybrid active power filter (TCLC-HAPF)," *IEEE Trans. Ind. Electron.*, vol. 69, no. 1, pp. 29–40, Jan. 2022.

Xuan Wu was born in Hunan, China, in 1983. He received the M.S. and Ph.D. degrees in automation from the College of Electrical and Information Engineering, Hunan University, Changsha, China, in 2011 and 2016, respectively.

He is an Associate Professor with the College of Electrical and Information Engineering, Hunan University. His research interests include permanent magnet synchronous motor drives and position sensorless control of AC motors.

Dan Yang was born in Hunan, China, in 1999. She received the B.S. degree in electrical and information engineering from the Changsha University of Science and Technology Changsha, China, in 2021. She is currently working toward the M.S. degree in electrical engineering with the College of Electrical and Information Engineering, Hunan University, Changsha, China.

Her current research interests include permanent magnet synchronous motor drive and position sensorless control.

Xu Yu was born in Hubei, China, in 1998. He received the B.S. degree in electrical and information engineering from the Changsha University of Science and Technology, Changsha, China, in 2020. He is currently working toward the Ph.D. degree in electrical engineering with the College of Electrical and Information Engineering, Hunan University, Changsha, China.

His current research interests include permanent magnet synchronous motor drive, position sensorless control, and dead-time compensation.

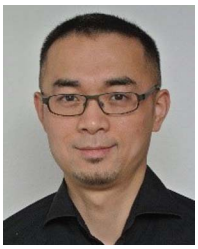

Kaiyuan Lu (Member, IEEE) received the B.S. and M.S. degrees from the Zhejiang University, Zhejiang, China, in 1997 and 2000, respectively, and the Ph.D. degree from the Aalborg University, Aalborg, Denmark, in 2005, all in electrical engineering.

In 2005, he became an Assistance Professor with the Department of Energy Technology, Aalborg University, where he has been an Associate Professor since 2008. His research interests include design of permanent magnet machines, finite element method analysis, and control of permanent magnet machines.

Ting Wu was born in Hunan, China, in 1994. She received the B.S. degree in electrical engineering from the Hunan Institute of Engineering, Xiangtan, China, in 2016, the M.S. and Ph.D. degrees in electrical engineering from Hunan University in 2018 and 2022, respectively.

She is currently a lecturer in School of Electronic Information, Hunan First Normal University, Changsha, China. Her current research interests include permanent magnet synchronous motor drive and position sensorless control of AC motors.

Shoudao Huang (Senior Member, IEEE) received the B.E. and Ph.D. degrees in electrical engineering from the Hunan University, Changsha, China, in 1982 and 2003, respectively.

He is currently a Professor with the College of Electrical and Information Engineering, Hunan University. His research interests include motor drives, power electronics, and control systems.

Hesong Cui was born in Heilongjiang, China. He received the B.S. degree in electrical engineering from the Harbin University of Science and Technology, Harbin, China in 2010, and the M.S. degree in electrical engineering from the Beihang University, Beijing, China, in 2016.

He is currently a Senior Engineer with the Machinery Industry Beijing Electrotechnical Institute of Economic Research, Beijing, China. His current research interests include motor drives and power electronics.